Scientific Reports

https://doi.org/10.1038/s41598-026-37989-8

Article in Press

Integrative metabolomic and single-cell transcriptomic analysis of recurrent condyloma acuminatum in humans

Received: 27 October 2025

Accepted: 28 January 2026

Published online: 04 February 2026

Cite this article as: Wei Y., Xu Y., Feng C. *et al.* Integrative metabolomic and single-cell transcriptomic analysis of recurrent condyloma acuminatum in humans. *Sci Rep* (2026). https://doi.org/10.1038/s41598-026-37989-8

Yushu Wei, Yaohan Xu, Chenxi Feng, Siji Chen, Jie Chen, Jiacheng Wang, Jingying Pan, Yinjing Song, Chunting Hua, Miaolian Cai, Hao Cheng & Jiang Zhu

Integrative Metabolomic and Single-Cell Transcriptomic Analysis of Recurrent Condyloma Acuminatum in Humans

Yushu Wei[1,#], Yaohan Xu [1,#], Chenxi Feng [1,#], Siji Chen[1], Jie Chen [1], Jiacheng Wang[1], Jingying Pan[1], Yinjing Song[1], Chunting Hua[1], Miaolian Cai[1], Hao Cheng[1,*], Jiang Zhu [1,*].

[1] Department of Dermatology and Venereology, Sir Run Run Shaw Hospital, Zhejiang University School of Medicine, Hangzhou 310016, P.R. China.

[#]These authors contributed equally.

[*]Corresponding author

Correspondence to:

Professor Jiang Zhu (Lead Corresponding Author): Department of Dermatology and Venereology, Sir Run Run Shaw Hospital, Zhejiang University School of Medicine, 3 Qingchun Road. Hangzhou 310016, P.R. China. Email: jzhu1@zju.edu.cn

Professor Hao Cheng: Department of Dermatology and Venereology, Sir Run Run Shaw Hospital, Zhejiang University School of Medicine, 3 Qingchun Road. Hangzhou 310016, P.R. China. Email: chenghao1@zju.edu.cn

Abbreviations: CA, condyloma acuminatum; HPV, human papillomavirus.

Keywords: condyloma acuminatum, human papillomavirus, recurrence, metabolomics, single-cell sequencing, immunometabolism

Running title: YUSHU WEI et al: METABOLOMIC AND SINGLE-CELL ANALYSES IN RECURRENT CONDYLOMA ACUMINATUM

Abstract

Condyloma acuminatum (CA), primarily caused by low-risk HPV6/11, is a benign proliferative disease that is difficult to cure and prone to recurrence. However, the molecular and immune mechanisms underlying relapse remain unclear. We combined metabolomic profiling with single-cell RNA sequencing to investigate recurrence-associated changes. Metabolomics revealed dysregulation of ascorbate and aldarate, glycerophospholipid, purine, and arginine/proline metabolism in recurrent CA. Single-cell analysis identified altered expression of metabolism-related genes (AMD1, GSTM3, ALDH3A1, GPX1, GPX4) in keratinocytes, associated with hyperproliferation, impaired differentiation, and ferroptosis resistance. Immune profiling identified transcriptionally distinct myeloid subpopulations in recurrent CA lesions, including M2 macrophages and dendritic cells. KEGG analysis indicated enrichment of antigen processing, phagosome, and endocytosis pathways in M2 macrophages, and antigen processing and viral carcinogenesis in dendritic cells, suggesting altered immune regulatory states. Notably, the key polyamine biosynthesis regulator AMD1 was downregulated in both M2 macrophages and dendritic cells in recurrent lesions, paralleling metabolic evidence of altered arginine-polyamine pathways. These findings suggest that recurrent CA involves coordinated metabolic dysregulation across keratinocytes and immune cells, highlighting potential targets for immunometabolic intervention.

Introduction

CA is a common sexually transmitted disease caused by HPV, with

about 90% of cases linked to HPV types 6 and 11[1]. CA presents as growths on the genitals and around the anus, with symptoms developing in approximately 65% of patients within 3 weeks to 8 months[1,2]. Although CA is not life-threatening, it can cause psychological distress and reduce quality of life. The prevalence of HPV infection is higher in developing countries, with Asia reporting the highest rates among women. Current treatment modalities include topical agents, laser therapy, cryotherapy, and interferon-based immune modulation, However, curing CA is challenging due to the high recurrence rates, often necessitating repeated treatments[2,3].

The pathogenesis of CA is complex, with HPV infection, particularly low-risk HPV types, being the primary risk factor[3]. Additional contributors include immunosuppression, high-risk sexual behavior, multiple sexual partners, and smoking[4,5]. HPV primarily targets keratinocytes in the basal layer of the skin and mucous membranes, entering cells via receptors such as heparan sulfate proteoglycans (HSPGs) and laminin-332 (LN332)[6–8]. After entry, the viral genome persists as an episome in the nucleus, replicating alongside host cell division[6]. HPV expresses its proteins through the coordinated regulation of the E and L genes, with the E gene primarily controlling keratinocyte proliferation and apoptosis. Notably, the E6 and E7 oncoproteins, products of the E gene, are critical for promoting cell proliferation and inhibiting apoptosis[9,10], leading to excessive proliferation of cells and the formation of warts in low-risk HPV infections[10,11]. The E6 and E7 oncoproteins play central roles in immune evasion by suppressing interferon signaling, downregulating antigen presentation, and dampening proinflammatory cytokine responses, which facilitates viral persistence[6,12]. L2 is largely concealed within the native virion

beneath the L1 capsid shell, which limits its exposure to neutralizing antibodies. Moreover, its role in mediating endosomal escape may indirectly contribute to evading intracellular immune detection during early infection[13,14]. However, current evidence does not establish a direct immune-modulatory function for L1 or L2, and further studies are needed to clarify whether these capsid proteins participate in immune evasion beyond their structural and trafficking roles. These mechanism allows HPV to persist in host cell for a long time, leading to chronic infection and the recurrence of CA. Despite these insights, the molecular regulatory networks between HPV and keratinocytes remain poorly understood, limiting therapeutic advancement. Therefore, further research into the molecular mechanisms of CA is crucial for advancing prevention and treatment strategies.

Metabolism is a fundamental process that sustains cellular life and represents a critical factor in the initiation and progression of viral infections[15]. The metabolic reprogramming not only facilitates viral proliferation but also influences host cell proliferation, differentiation, and immune responses[16,17]. Studies have shown that HPV infection can enhance glucose metabolism and energy supply in local epithelial cells, weaken local immune clearance capabilities, and promote viral latency and reactivation by maintaining an abnormal metabolic microenvironment[18,19]. However, most studies focus on anogenital cancers caused by high-risk types of HPV[20,21], with limited research on CA or low-risk HPV infections, particularly regarding the molecular interactions within keratinocytes. While HPV molecular mechanisms are partially understood, the metabolic and transcriptional drivers of CA recurrence remain unexplored.

In this study, we integrated single-cell sequencing and metabolomic analyses to investigate the molecular mechanisms

underlying the pathogenesis and recurrence of CA. By combining these complementary approaches, we characterized metabolic and transcriptional alterations in the skin of patients with recurrent CA compared with healthy controls. This integrative strategy enabled systematic analysis of recurrence-associated metabolic pathways and gene expression networks, as well as the interactions between keratinocytes and immune cells within the local microenvironment. Ultimately, our aim was to identify molecular signatures and potential therapeutic targets that may inform improved strategies for the prevention and treatment of CA.

2. Materials and methods

2.1 Untargeted metabolomics sample collection

Foreskin, perianal and vulva samples were collected from 11 primary CA patients, 6 recurrent CA patients, and 10 healthy controls admitted to Sir Run Run Shaw Hospital (Hangzhou, China) between April 2017 and September 2023. All patients provided written informed consent before participating in this study, in accordance with the Declaration of Helsinki and institutional ethical guidelines. This study was approved by the Medical Ethics Committee of Sir Run Run Shaw Hospital, Zhejiang University School of Medicine under approval number 20210330-39.

Recurrent CA was defined as the reappearance of clinically visible anogenital warts at the same or adjacent sites within 3-12 months after complete resolution following standard treatments such as intralesional interferon, photodynamic therapy, or microwave ablation. All recurrent patients had at least one prior episode of CA. Patients with immunodeficiency, chronic systemic disease, or concurrent sexually transmitted infections were excluded. Detailed clinical information and HPV type for each sample are summarized in Supplementary Table S1.

2.2 Metabolomics analysis

Metabolomic analysis was performed using a Triple TOF 5600 Plus high-resolution tandem mass spectrometer (MS/MS; SCIEX, Warrington, United Kingdom) operating in both positive and negative ion modes. Chromatographic separation was conducted using an ultra-performance liquid chromatography (UPLC) system (SCIEX, United Kingdom). LC-MS data preprocessing was performed using XCMS software. Untargeted metabolomic analyses were carried out by LC-Bio (Hangzhou, China). Metabolite set enrichment analysis (MSEA) and KEGG pathway enrichment analysis were conducted using MetaboAnalyst (https://www.metaboanalyst.ca/), with pathway annotation and functional mapping based on the KEGG database[22–24].

Raw LC-MS peak area data were imported into MetaboAnalyst 5.0 for processing. Metabolite intensities were normalized by total ion current (TIC) to correct for variation in signal intensity among samples, $\log_2$-transformed, and auto-scaled (mean-centered and divided by the standard deviation of each variable) before statistical and pathway analyses. Normalized metabolite levels of representative metabolites from key KEGG pathways were exported from MetaboAnalyst and visualized using GraphPad Prism 8 for bar plot generation and statistical comparison.

2.3 Clinical sample collection, and preparation of single-cell suspensions

Foreskin and perianal samples were collected from 4 recurrent CA patients, and 4 healthy controls. They were admitted to the Sir Run Run Shaw Hospital (Hangzhou, China) between July 2020 and October 2020. Detailed clinical information and HPV type for each sample are summarized in Supplementary Table S2 and Supplementary Table S3. The criteria for recurrent CA were

identical to those described in Section 2.1.

Place a sterile RNase-free culture dish containing an appropriate amount of calcium-free and magnesium-free 1 × PBS on ice, the tissue was transferred into the culture dish and cut it into 0.5 mm^2 pieces, the tissues were washed with 1 × PBS, to remove as many non-purpose tissues as possible such as blood stains and fatty layers. Tissues were dissociated into single cells in dissociation solution (0.35% collagenase IV5,2 mg/ml papain, 120 Units/ml DNase I) in 37 ℃ water bath with shaking for 20 min at 100 rpm. Digestion was terminated with 1× PBS containing 10% fetal bovine serum (FBS□V/V), then pipetting 5-10 times with a Pasteur pipette. The resulting cell suspension was filtered by passing through 70-30 um stacked cell strainer and centrifuged at 300g for 5 min at 4 °C. The cell pellet was resuspended in 100ul 1× PBS (0.04% BSA) and added with 1 ml 1× red blood cell lysis buffer （MACS 130-094-183, 10×）and incubated at room temperature or on ice for 2-10 min to lyse remaining red blood cells. After incubation, the suspension was centrifuged at 300g for 5 min at room temperature. The suspension was resuspended in 100 μl Dead Cell Removal MicroBeads (ACS 130-090-101) and remove dead cells using Miltenyi ® Dead Cell Removal Kit (MACS 130-090-101). Then the suspension was resuspended in 1× PBS(0.04% BSA) and centrifuged at 300 g for 3 min at 4 °C（repeat twice）. The cell pellet was resuspended in 50 μl of 1× PBS (0.04% BSA). The overall cell viability was confirmed by trypan blue exclusion , which needed to be above 85%, single cell suspensions were counted using a Countess II Automated Cell Counter and concentration adjusted to 700-1200 cells/μl. Following single-cell suspension preparation, libraries were constructed for transcriptomic profiling.

2.4 Chromium 10x Genomics library, sequencing and

bioinformatics analysis

Single-cell suspensions were counted and loaded onto the Chromium Single Cell 3’ Chip (10× Genomics) according to manufacturer’s instructions for the 10× Genomics Chromium Single-Cell 3’ kit v3. The 12 10×reactions were distributed across 5 chips, with each reaction involving the following number of cells: 7199 (CA_1), 7044 (GHP4), 12578 (I3107_1), 8774 (three), 8346 (HP1), 6794 (HP2), 5783 (HP3), and 6003 (HP4). The following cDNA amplification and library construction steps were performed according to the standard protocol. Libraries were sequenced on an Illumina NovaSeq 6000 sequencing system (paired-end multiplexing run, 150bp) by LC-Bio Technology co.ltd., (HangZhou, China) at a minimum depth of 20,000 reads per cell.

To visualize the data, we further reduced the dimensionality of all 56518 cells using Seurat and used t-SNE to project the cells into 2D space, The steps includes: Using the LogNormalize method of the "Normalization" function of the Seurat software to calculated the expression value of genes; PCA (Principal component analysis) analysis was performed using the normalized expression value, Within all the PCs, the top 10 PCs were used to do clustering and t-SNE analysis; To find clusters, selecting weighted Shared Nearest Neighbor (SNN) graph-based clustering method. Marker genes for each cluster were identified with the "bimod" （Likelihood-ratio test）with default parameters via the FindAllMarkers function in Seurat. Marker genes were defined as those expressed in more than 10% of the cells within a cluster and exhibiting an average log fold change greater than 0.26.

2.5 Differential expression gene (DEG) and Kyoto Encyclopedia of Genes and Genomes KEGG analysis

Differentially expressed genes (DEGs) were identified using the

Seurat R package with the FindAllMarkers function based on the bimod likelihood-ratio test. For each comparison, p-values were adjusted for multiple testing using the Benjamini-Hochberg method, and genes with |log2 fold change| > 1 and adjusted p-value (FDR) ≤ 0.05 were considered statistically significant. KEGG pathway enrichment analysis was conducted on http://www.genome.jp/kegg/ with FDR < 0.05[22,24].

2.6 Chemicals and reagents

AMD1 Polyclonal antibody (Proteintech, Cat# 11052-1-AP), GSTM3 Polyclonal antibody (Proteintech, Cat# 15214-1-AP), ALDH3A1 Polyclonal antibody (Proteintech, Cat# 15578-1-AP), GPX4 Monoclonal antibody (Proteintech, Cat# 67763-1-Ig), and RRM2 Polyclonal antibody (Proteintech, Cat# 11661-1-AP) were purchased from Proteintech (Chicago, IL, USA). All antibodies were validated for human tissue applications and used for both immunohistochemistry and immunofluorescence assays as described in Section 2.7.

2.7 Immunohistochemistry (IHC) and Immunofluorescence (IF) staining

Formalin-fixed paraffin-embedded (FFPE) tissue sections (4 μm thick) from recurrent CA lesions and control samples were deparaffinized in xylene and rehydrated through graded ethanol. Antigen retrieval was performed in citrate buffer (pH 6.0) at 95 °C for 20 min. Endogenous peroxidase activity was quenched with 3% hydrogen peroxide for 10 min, followed by blocking in 5% bovine serum albumin (BSA) for 30 min at room temperature.

Primary antibodies were incubated overnight at 4 °C, followed by incubation with horseradish peroxidase (HRP)-conjugated secondary antibodies (ZSGB-BIO, Beijing, China) for 1 h at room temperature. Staining was visualized using diaminobenzidine (DAB)

substrate and counterstained with hematoxylin. Slides were scanned using a Leica DM4000 microscope. Quantitative analysis was performed with ImageJ software by measuring the average optical density (AOD) from at least five randomly selected fields per section.

For immunofluorescence (IF) staining, sections were blocked with 5% BSA for 30 min and incubated with primary antibodies overnight at 4 °C, followed by fluorophore-conjugated secondary antibodies (Alexa Fluor 488/594, Invitrogen) for 1 h at room temperature. Nuclei were counterstained with DAPI (Beyotime, China). Fluorescence images were captured using a Zeiss LSM 880 confocal microscope. Fluorescence intensity was quantified using ImageJ (integrated density normalized to DAPI area).

2.8 Quantification Statistical analysis

GraphPad Prism 8 was used for data analysis, and measurement data were expressed as the mean ± standard deviation (mean ± SD). Upaired T-test, Welch's test and Mann-Whitney test were used for comparisons between two groups of data. Statistical significance was set at $P < 0.05$.

3.Results

3.1Analysis of total metabolites in recurrent CA patients

To explore the pathogenesis of CA, we performed metabolomic analyses on skin tissue samples from 6 patients with recurrent CA, 11 with primary CA, and 10 healthy controls. As shown in **Figure 1A**, 381 metabolites were differentially expressed between primary patients and healthy controls, 228 between recurrent patients and healthy controls, and 33 between recurrent and primary patients. In primary patients compared to healthy controls, 163 metabolites were upregulated and 218 downregulated; in recurrent patients, 103 metabolites were upregulated and 125

downregulated relative to healthy controls. Notably, 10 metabolites were upregulated and 23 downregulated in recurrent compared to primary patients. The 33 metabolites unique to recurrent CA suggest distinct metabolic reprogramming during relapse. In addition, the volcano plot revealed significant metabolites dysregulations (**Figure 1B and 1C**). The heatmap (**Figure 1D**) showed the 30 most significantly dysregulated metabolites between recurrent patients and healthy controls. Among these, Inosine 5'-monophosphate, Inosinic acid and Adenosine 5'-monophosphate showed the greatest upregulation, whereas cytidine, 3-Acetylindole and D-2-Phosphoglyceric acid showed the most significant downregulation. Our findings reveal significant metabolic dysregulation in recurrent CA patients compared to healthy controls. These altered metabolites may serve as potential biomarkers for disease detection or therapeutic intervention. Modulating their levels could facilitate earlier diagnosis and inform novel treatment strategies. To further investigate their functional relevance, we conducted KEGG pathway analysis.

3.2 KEGG enrichment analysis of metabolites between recurrent CA patients and healthy controls

To better understand the biological basis of CA, we performed Kyoto Encyclopedia of Genes and Genomes (KEGG) pathway analysis on metabolites between recurrent patients and healthy controls. As shown in **Figure 2A**, significant alterations were observed in multiple metabolic pathways, particularly glycerophospholipid metabolism, nucleotide metabolism, teichoic acid biosynthesis, and autophagy. KEGG enrichment analysis was conducted on metabolites exhibiting significant differences between recurrent patients and healthy controls, and four

pathways with the lowest p-values and highest pathway impact were selected for further analysis (**Figure 2B**). In purine metabolism, inosine 5'-monophosphate and AMP were the two most significantly upregulated metabolites, while guanine was notably downregulated (**Figure 2C and D**). In ascorbate and aldarate metabolism, UDP-D-Glucuronic acid was significantly upregulated, and myo-Inositol was significantly downregulated (**Figure 2C and E**). In glycerophospholipid metabolism, LysoPE 16:1, LysoPC 16:1, LysoPS 16:1; LysoPS 16:1 were the most significantly upregulated metabolites, and LysoPG 22:5; LysoPG 22:5, PG 36:4; PG (18:2/18:2), sn-Glycero-3-phosphocholine were the most significantly downregulated metabolites (**Figure 2C and F**). In arginine and proline metabolism, S-Adenosyl-L-methionine, N-Acetylputrescine and putrescine were significantly upregulated (**Figure 2C and G**). These findings suggest that metabolic alterations may contribute to CA recurrence, underscoring the role of metabolic regulation in disease progression and providing a basis for future mechanistic and therapeutic investigations.

3.3 Single-cell sequencing of skin biopsy specimens in recurrent CA patients and healthy controls detects multiple skin cell clusters

We investigated skin samples from four recurrent CA patients and compared them to four matched healthy controls. After high-quality filtering, 62521 cells were included in further analyses (Recurrence group, 35595 cells; Control group, 26926 cells). Using t-SNE for dimensionality reduction, we visualized the clustering of seven distinct cell types: keratinocytes (KC), T cells, endothelial cells, fibroblasts, myeloid cells, pericytes and melanocytes **(Figure 3A)**. Cell type assignments were validated by canonical marker: Keratinocytes expressed KRT14, KRT10, and KLF5; T cells

were marked by CD3G, CD3E, and CD3D; Endothelial cells expressed PECAM1, CDH5, and VWF; Fibroblasts were characterized by DCN, COL1A1, and COL3A1; Myeloid cells expressed CSF1R, CD163, and LYZ; Pericytes were marked by ACTA2 and RGS5; Melanocytes expressed TYR, TYRP1, and MLANA[21,25,26] **(Figure 3B)**. Keratinocytes were the predominant cell type, while T cells and myeloid cells largely comprised the immune microenvironment **(Figure 3B)**.

As HPV primarily infects keratinocytes, we further dissected KC subpopulations to identify recurrence-associated alterations. Subsequent analysis focused on keratinocytes (KC), which were subdivided into five subgroups: Basal KC (marked by COL17A1, KRT15, KRT5), Late-differentiated KC (CDSN, FLG, LOR), Proliferating KC (PTTG1, RRM2, HELLS, TK1), Spinous cells (DEFB1, FXYD3), and Suprabasal KC (KRT1, KRT10, KRTDAP) **(Figures 3C, 3D)**[27].

In **Figure 3E**, we compared the cell composition between recurrent CA patients and controls, revealing a significant increase in the proportion of basal KC (p = 0.028) and a significant decrease in late-differentiated KC (p = 0.028) in recurrent CA patients. The expansion of basal KCs—a progenitor compartment—may reflect HPV-driven epidermal hyperproliferation in recurrent lesions. We then assessed the expression of metabolism-associated genes in both groups. **Figure 3F** presents the overall gene expression profiles of skin tissues from these two cohorts, showing differential expression of several genes, including KRT1, KRT16, KRT17, KRT6A, KRT6B, KRT6C, FABP5, CXCL14, and S100A9. These genes may be implicated in the pathogenesis of CA, offering valuable insights into the disease's molecular mechanisms and potential

therapeutic targets or biomarkers.

3.4 KEGG pathway analysis of genes expressed in KC of recurrent CA patients from single-cell sequencing results

We performed Kyoto Encyclopedia of Genes and Genomes (KEGG) pathway analysis on genes expressed in KC in recurrence VS control group **(Figure 4A)**. Several pathways exhibited high enrichment factors and low *p* values, including Parkinson's disease (hsa05012), oxidative phosphorylation (hsa00190), Huntington's disease (hsa05016), thermogenesis (hsa04714), ribosome (hsa03010), and proteasome (hsa03050). **Figure 4B** highlights the twelve most significantly altered pathways, with glycolysis/gluconeogenesis, glutathione metabolism, and pyrimidine metabolism being the top three most significantly affected metabolic pathways.

3.5 Gene expression changes in glycolysis/gluconeogenesis, glutathione, and pyrimidine metabolism in KC of recurrent CA patients

In glycolysis/gluconeogenesis signaling pathway, 10 genes (including ENO1, AKR1A1, ADH5, PGK1, LDHA, PGAM1, GAPDH, TPI1, LDHB, PKM) were significantly up-regulated and 3 genes (including ALDH3A1, ALDH3A2, ALDH3B2) were significantly down-regulated in recurrent patients **(Figure 5A)**. **Figure 5D** shows the expression of these genes across different KC subclusters. In glutathione metabolism, 8 genes (including SRM, ODC1, GPX1, GSTP1, GSTO1, MGST1, GPX2, GPX4) were significantly up-regulated and 3 genes (including GSTM3, GSTA3, GGT6) were significantly down-regulated in recurrent patients **(Figure 5B)**. **Figure 5E** illustrates their expression in various KC subclusters. In pyrimidine metabolism, 11 genes (including CDA, DTYMK, UPP1, DUT, NME3, DCTPP1, NME1, NT5C, TK1, TYMS,

TYMP)were significantly up-regulated in recurrent patients **(Figure 5C)**, with their expression also depicted in different KC subclusters in **Figure 5F**.

3.6 Gene expression changes in arginine and proline metabolism, purine metabolism in KC of recurrent CA patients

We integrated metabolomics and single-cell sequencing data and identified significant alterations in arginine and proline metabolism, as well as purine metabolism, in both datasets **(Figures 2 and 4)**. In arginine and proline metabolism, 3 genes (SRM, ODC1, GAMT) were significantly upregulated, while 3 genes (AMD1, MAOA, ALDH3A2) were downregulated in recurrent patients **(Figure 6A)**. **Figure 6B** illustrates the expression of these genes across different KC subclusters. In purine metabolism, 8 genes (AK2, GUK1, NUDT5, PKM, NME3, NME1, NT5C, ITPA) were significantly upregulated in recurrent patients **(Figure 6C)**, with their expression across KC subclusters shown in **Figure 6D**.

3.7 The expression changes of AMD1, GSTM3, ALDH3A1, GPX4, GPX1 in recurrent CA patients

We integrated transcriptomic data from recurrent CA patients with genes detected via single-cell sequencing, identifying 10 shared genes: UPP1, AKR1B10, AMD1, GSTM3, ECHS1, ALDH3A1, MDH2, GPX4, GPX1, and AKR1B1. Then, we used the pathways-related genes mentioned above to screen these genes and finally selected 5 target genes: AMD1, GSTM3, ALDH3A1, GPX4, GPX1. Expression of these genes varied across different KC clusters, with significant changes observed in basal KC, late-differentiated KC, and proliferating KC **(Figure 5 and Figure 6)**.

The AMD1 gene (involved in arginine and proline metabolism)

was significantly downregulated in recurrent CA patients, particularly in basal and late-differentiated KC. GSTM3 (involved in glutathione metabolism) was downregulated, especially in basal and proliferating KC. ALDH3A1 (involved in glycolysis/gluconeogenesis) was also downregulated, particularly in basal and proliferating KC. In contrast, both GPX4 and GPX1 (involved in glutathione metabolism) were upregulated in recurrent patients, with GPX4 showing significant changes in proliferating KC and GPX1 in basal and proliferating KC.

3.8 Single-cell analysis reveals M2 macrophage enrichment and dendritic cell dysfunction in recurrent CA

To investigate CA-associated immune mechanisms, we dissected myeloid subpopulations to identify recurrence-associated alterations **(Figure 7A and B)**. Subsequent analysis focused on M2 macrophages (marked by CXCL8, CCL22, MRC1) and dendritic cells (marked by GADD45A, NR4A2, IRF8). KEGG pathway analysis of M2 macrophages in recurrent vs. control groups showed strong enrichment (high enrichment factor, low p-value) for antigen processing and presentation (hsa04612), phagosome (hsa04145), and endocytosis (hsa04144) **(Figure 7C)**, implicating these processes in recurrence. A heatmap highlighted differentially expressed genes linked to these pathways **(Figure 7D)**. Parallel analysis in dendritic cells identified enriched pathways including antigen processing and presentation (hsa04612) and viral carcinogenesis (hsa05203) **(Figure 7E)**. A corresponding heatmap displayed key genes associated with these processes **(Figure 7F)**.

In addition, we examined the expression of key enzymes involved in polyamine metabolism within immune subsets. Among these, AMD1 (S-adenosylmethionine decarboxylase 1), which catalyzes a rate-limiting step in putrescine synthesis, was

significantly downregulated in M2 macrophages and dendritic cells from recurrent CA lesions compared with controls (Supplementary Tables S4 and S5).

3.9 Immunohistochemical and immunofluorescence analysis of AMD1, GSTM3, ALDH3A1, GPX4, and RRM2 expression in recurrent CA patients

We investigated the expression of AMD1 **(Figure 8A)**, GSTM3 **(Figure 8B)**, ALDH3A1 **(Figure 8C)**, and GPX4 **(Figure 8D)** in recurrent CA patients and healthy controls using immunohistochemistry, followed by quantitative analysis. The results showed that AMD1, GSTM3, and ALDH3A1 were significantly downregulated in recurrent CA patients ($p < 0.01$), while GPX4 was notably upregulated ($p < 0.05$) **(Figure 8E)**. Additionally, immunofluorescence staining of DAPI, GPX4, and RRM2 (a marker for proliferating KC) revealed upregulation of all three in recurrent CA patients **(Figure 8F)**.

The immunohistochemistry and immunofluorescence results were highly consistent with those from single-cell sequencing and metabolomics, supporting the proposed therapeutic targets for CA.

Discussion

This study provides new molecular insights into the pathogenesis and recurrence of CA by integrating metabolomic and single-cell transcriptomic analyses. Previous studies have identified several immunomarkers and genes associated with CA pathogenesis. For instance, GZMB, IFNG, IL8, and IL12B were upregulated, while NFATC4 and IL7 were downregulated in CA patients[5]. In our study, purine metabolism, ascorbate and aldarate metabolism, glycerophospholipid metabolism, and arginine and proline metabolism were notably altered in CA patients. Additionally, recurrent cases showed dysregulation of genes including AMD1,

GSTM3, ALDH3A1, GPX4, and GPX1.

Arginine and proline metabolism is critical in cellular amino acid metabolism, supporting functions like energy metabolism, antioxidation and protein synthesis. Arginine is converted into putrescine and other polyamines (e.g., spermidine, spermine), which are essential for cell growth and differentiation. During tissue growth, wound repair, and immune responses, elevated arginine levels promote putrescine synthesis, driving cell proliferation and differentiation. This pathway is particularly vital in rapidly dividing cells, such as immune, epithelial, and muscle cells[28–32]. Among the key enzymes in this pathway, AMD1 (S-adenosylmethionine decarboxylase 1) catalyzes the decarboxylation of S-adenosylmethionine, generating aminopropyl groups required for spermidine and spermine synthesis. Previous studies have shown that decreased AMD1 expression leads to reduced spermine levels and increased putrescine accumulation, resulting in excessive keratinocyte proliferation and impaired differentiation[28,32].

In our study, AMD1 expression was significantly reduced in recurrent CA lesions, accompanied by elevated levels of S-adenosyl-L-methionine, N-acetylputrescine, and putrescine. Notably, AMD1 downregulation was consistently observed in keratinocytes, M2 macrophages, and dendritic cells based on our integrated single-cell transcriptomic and metabolomic analyses. These findings suggest a disturbance of the arginine-polyamine metabolic axis in both epithelial and immune compartments. While the overall proportions of M2 macrophages and dendritic cells did not differ significantly between groups, transcriptional alterations within these subsets imply a state of metabolic reprogramming, potentially influencing local immune regulation. Given that M2 macrophages drive polyamine production through the ARG1

pathway[33–35], they may contribute to the altered polyamine milieu observed in recurrent CA. The resulting accumulation of putrescine could create a hyperproliferative and differentiation-impaired epithelial microenvironment conducive to lesion persistence. Therapeutically, modulation of the AMD-polyamine axis may represent a promising approach to restore epithelial homeostasis and prevent recurrence. Further metabolic flux and functional studies are warranted to substantiate these mechanisms.

We observed significant upregulation of the GPX4 and GPX1 genes, both involved in glutathione metabolism, in recurrent CA patients, while GSTM3 expression was notably downregulated. GPX1, a crucial antioxidant enzyme, mitigates oxidative stress by regulating intracellular ROS and maintaining redox balance. Its overexpression in various cancers enhances tumor proliferation, invasion, migration, apoptosis resistance, immune evasion, and drug resistance, thereby serving as a promising prognostic biomarker linked to clinicopathological features[36,37]. GPX4, detoxify lipid hydroperoxides using glutathione (GSH) as a cofactor, thus shielding cells from lipid peroxidation and ferroptosis, a process that is especially critical in HPV-related cancers[38]. Among the various isoenzymes, GPX4 exists as a monomer and is easy to inhibit. In anticancer drug screenings, agents like ML162, RSL3 and ML210 have been found to inhibit GPX4, inducing ferroptosis[39,40]. Studies show that GSTM3 contributes to tumorigenesis and cancer progression, partly by modulating ferroptosis through GPX4. Lower GSTM3 expression is associated with tumor recurrence and poorer prognosis[41,42]. Therefore, targeting GPX1 and GPX4, activating GSTM3, and modulating glutathione metabolism could represent potential therapeutic strategies for CA. Besides, the poor solubility, low permeability, and rapid metabolic clearance of GPX4 inhibitors may

limit the effectiveness of systemic administration[43], suggesting that topical formulations could be more effective. Nonetheless, the exact molecular mechanism linking these genes to CA needs further exploration.

We found that the ALDH3A1 gene, involved in glycolysis/gluconeogenesis, was significantly downregulated in recurrent CA patients. Studies have shown that targeting glycogen metabolism, such as inhibiting glycogen phosphorylase, is a promising therapeutic strategy for diseases with hyperactive glycogen metabolism, including cervical carcinoma[44,45]. Furthermore, glycolysis and glycogen metabolism are significantly upregulated in keratinocytes infected with low-risk HPV in CA[46]. Based on this, we suggest that inhibiting glycolysis/gluconeogenesis and modulating related genes like ALDH3A1 could offer potential therapeutic approaches for CA. RRM2, a specific marker of proliferating KC, is upregulated in recurrent CA patients, indicating increased KC proliferation. The upregulation of purine metabolites (e.g., AMP) aligns with increased RRM2 expression in proliferating KCs, suggesting enhanced nucleotide synthesis supports wart regrowth. RRM2 expression is known to be elevated in HPV infections. Thus, RRM2 may serve as a potential therapeutic target for CA[47,48].

In this study, we identified a significant expansion of basal keratinocytes accompanied by a reduction in late-differentiated keratinocytes in recurrent condyloma acuminatum (CA) lesions, indicating a shift toward a more proliferative and less differentiated epithelial state. While causality cannot be inferred, these findings are consistent with the established tropism of HPV for basal keratinocytes and its capacity to disrupt normal keratinocyte differentiation. As samples were collected from local lesions after

clinical recurrence, our results primarily reflect tissue-level metabolic and transcriptional features associated with recurrence rather than initiating or causal mechanisms. Direct comparison between recurrent and non-recurrent CA remains challenging because primary CA is biologically heterogeneous and recurrence status can only be determined through longitudinal follow-up. Additional limitations include small sample sizes in metabolomic (n=6) and single-cell RNA-sequencing (n=4) analyses, limited tissue availability, and stringent cell viability requirements. Despite these constraints, the data quality supported exploratory analyses and provided an initial characterization of the cellular and immunometabolic landscape of recurrent CA. These findings should be interpreted cautiously and validated in larger, longitudinal cohorts with well-defined non-recurrent populations.

Conclusion

This study combined metabolomic and single-cell sequencing analyses to explore gene, metabolic pathway, and metabolite interactions in CA lesions, especially in recurrent cases. We identified key changes in metabolites and genes that may regulate CA initiation and recurrence, offering new insights into potential therapeutic targets.

Acknowledgements

We sincerely thank all the patients and healthy volunteers who generously participated in this study. We are also deeply grateful to all colleagues and collaborators at the Department of Dermatology and Venereology, Sir Run Run Shaw Hospital, Zhejiang University School of Medicine, for their valuable support throughout the research process. Additionally, we acknowledge the contributions of Hangzhou LC-BIO Co., Ltd., for their technical assistance in

sequencing and bioinformatics analysis.

Author contribution statement

Y.W., Y.X., C.F., J.Z, and Y.S. conceived and designed the study. Y.W., Y.X., S.C., J.P., J.W. and J.C. performed the experiments. Y.X., J.Z., S.C., J.P., J.C., J.W. and C.F. analyzed the data. Y.W., H.C., and J.Z. wrote and reviewed the manuscript. C.H. and M.C. assisted in manuscript revision and figure preparation. Y.S., H.C., and J.Z. assume overall responsibility for the manuscript. J.Z., and H.C., were responsible for supervision and funding acquisition.

Data availability

All sequencing data supporting the findings of this study have been deposited in the Genome Sequence Archive database under accession number HRA009671 and are available at the following URL: https://ngdc.cncb.ac.cn/gsa-human/s/n6wYVK0Q. Additional data are available from the corresponding author upon reasonable request.

Conflict of interest

All authors declare no conflicts of interest. We have not received funding or support from any sponsor, pharmaceutical company, or other organization. Any potential conflicts, if present, have been disclosed to the study participants. We had full access to all data, and the corresponding author assumes full responsibility for its accuracy.

Ethics approval and consent to participate

This study was approved by the Ethics Committee of Sir Run Run Shaw Hospital, Zhejiang University School of Medicine (Approval No. 20210330-39), and was conducted in accordance with the principles of the Declaration of Helsinki. All procedures involving human participants adhered to the institutional guidelines and were approved by the relevant ethics board. Written informed consent

was obtained from all participants prior to their inclusion in the study.

Patient consent for publication

All participants provided written informed consent for the publication of anonymized data and results derived from this study.

Funding information

This study was funded by grants from the Natural Science Foundation of China (82373491, 82471846, 82404156), and Zhejiang Provincial Natural Science Foundation of China (LY24H110001) . All authors have reviewed and approved the final manuscript.

Reference

1. Azevedo, J. *et al.* Epidemiology of human papillomavirus on anogenital warts in Portugal – The HERCOLES study. *Acad Dermatol Venereol* **31**, 1342–1348 (2017).
2. Patel, H., Wagner, M., Singhal, P. & Kothari, S. Systematic review of the incidence and prevalence of genital warts. *BMC Infect Dis* **13**, 39 (2013).
3. Ault, K. A. Epidemiology and natural history of human papillomavirus infections in the female genital tract. *Infect Dis Obstet Gynecol* **2006 Suppl**, 40470 (2006).
4. Sindhuja, T., Bhari, N. & Gupta, S. Asian guidelines for condyloma acuminatum. *J Infect Chemother* **28**, 845–852 (2022).
5. Stuqui, B. *et al.* Condyloma acuminata: An evaluation of the immune response at cellular and molecular levels. *PLoS ONE* **18**, e0284296

(2023).

6. Moody, C. A. & Laimins, L. A. Human papillomavirus oncoproteins: pathways to transformation. *Nat Rev Cancer* **10**, 550–560 (2010).
7. Harden, M. E. & Munger, K. Human papillomavirus molecular biology. *Mutat Res Rev Mutat Res* **772**, 3–12 (2017).
8. Ullah, M. I. *et al.* Molecular pathways in the development of HPV-induced oropharyngeal cancer. *Cell Commun Signal* **21**, 351 (2023).
9. Pinatti, L. M., Walline, H. M. & Carey, T. E. Human Papillomavirus Genome Integration and Head and Neck Cancer. *J Dent Res* **97**, 691–700 (2018).
10. Scheffner, M., Werness, B. A., Huibregtse, J. M., Levine, A. J. & Howley, P. M. The E6 oncoprotein encoded by human papillomavirus types 16 and 18 promotes the degradation of p53. *Cell* **63**, 1129–1136 (1990).
11. Huh, K.-W. *et al.* Association of the human papillomavirus type 16 E7 oncoprotein with the 600-kDa retinoblastoma protein-associated factor, p600. *Proc Natl Acad Sci U S A* **102**, 11492–11497 (2005).
12. Scarth, J. A., Patterson, M. R., Morgan, E. L. & Macdonald, A. The human papillomavirus oncoproteins: a review of the host pathways targeted on the road to transformation. *Journal of General Virology* **102**, (2021).
13. Jain, M. *et al.* Epidemiology, Molecular Pathogenesis, Immuno-Pathogenesis, Immune Escape Mechanisms and Vaccine Evaluation for HPV-Associated Carcinogenesis. *Pathogens* **12**, 1380

(2023).

14. Wang, J. W. & Roden, R. B. S. L2, the minor capsid protein of papillomavirus. *Virology* **445**, 175–186 (2013).
15. Thaker, S. K., Ch'ng, J. & Christofk, H. R. Viral hijacking of cellular metabolism. *BMC Biol* **17**, 59 (2019).
16. Lévy, P. & Bartosch, B. Metabolic reprogramming: a hallmark of viral oncogenesis. *Oncogene* **35**, 4155–4164 (2016).
17. Sanchez, E. L. & Lagunoff, M. Viral activation of cellular metabolism. *Virology* **479–480**, 609–618 (2015).
18. Sitarz, K., Czamara, K., Szostek, S. & Kaczor, A. The impact of HPV infection on human glycogen and lipid metabolism - a review. *Biochim Biophys Acta Rev Cancer* **1877**, 188646 (2022).
19. Gore, M., Kabekkodu, S. P. & Chakrabarty, S. Exploring the metabolic alterations in cervical cancer induced by HPV oncoproteins: From mechanisms to therapeutic targets. *Biochim Biophys Acta Rev Cancer* **1880**, 189292 (2025).
20. Singh, R. Single-Cell Sequencing in Human Genital Infections. in *Single-cell Sequencing and Methylation* (eds Yu, B., Zhang, J., Zeng, Y., Li, L. & Wang, X.) vol. 1255 203–220 (Springer Singapore, Singapore, 2020).
21. Guo, C. *et al.* Spatiotemporally deciphering the mysterious mechanism of persistent HPV-induced malignant transition and immune remodelling from HPV-infected normal cervix, precancer to cervical cancer:

Integrating single-cell RNA-sequencing and spatial transcriptome. *Clin Transl Med* **13**, e1219 (2023).

22. Kanehisa, M., Furumichi, M., Sato, Y., Matsuura, Y. & Ishiguro-Watanabe, M. KEGG: biological systems database as a model of the real world. *Nucleic Acids Res* **53**, D672–D677 (2025).
23. Kanehisa, M. Toward understanding the origin and evolution of cellular organisms. *Protein Science* **28**, 1947–1951 (2019).
24. Kanehisa, M. & Goto, S. KEGG: Kyoto Encyclopedia of Genes and Genomes. *Nucleic Acids Res* **28**, 27–30 (2000).
25. Qiu, J. *et al.* Single-Cell Landscape Highlights Heterogenous Microenvironment, Novel Immune Reaction Patterns, Potential Biomarkers and Unique Therapeutic Strategies of Cervical Squamous Carcinoma, Human Papillomavirus-Associated (HPVA) and Non-HPVA Adenocarcinoma. *Adv Sci (Weinh)* **10**, e2204951 (2023).
26. Wei, E. *et al.* Integration of scRNA-Seq and TCGA RNA-Seq to Analyze the Heterogeneity of HPV+ and HPV- Cervical Cancer Immune Cells and Establish Molecular Risk Models. *Front Oncol* **12**, 860900 (2022).
27. Zhou, J. *et al.* Single-cell RNA-seq reveals abnormal differentiation of keratinocytes and increased inflammatory differentiated keratinocytes in atopic dermatitis. *J Eur Acad Dermatol Venereol* **37**, 2336–2348 (2023).
28. Rahim, A. B. *et al.* The Polyamine Regulator AMD1 Upregulates Spermine Levels to Drive Epidermal Differentiation. *J Invest Dermatol* **141**,

2178-2188.e6 (2021).

29. Casero, R. A. & Marton, L. J. Targeting polyamine metabolism and function in cancer and other hyperproliferative diseases. *Nat Rev Drug Discov* **6**, 373–390 (2007).
30. Allmeroth, K. & Denzel, M. S. The RATIOnal Role of Polyamines in Epidermal Differentiation. *J Invest Dermatol* **141**, 2105–2107 (2021).
31. Pegg, A. E. Functions of Polyamines in Mammals *. *Journal of Biological Chemistry* **291**, 14904–14912 (2016).
32. Broshtilova, V., Lozanov, V. & Miteva, L. Comparative analysis of polyamine metabolism in benign and neoplastic keratinocytic proliferations. *Acta Dermatovenerol Alp Pannonica Adriat* **21**, 3–5 (2012).
33. Gorvel, L. & Olive, D. Tumor associated macrophage in HPV+ tumors: Between immunosuppression and inflammation. *Semin Immunol* **65**, 101671 (2023).
34. Li, M. *et al.* Metabolism, metabolites, and macrophages in cancer. *J Hematol Oncol* **16**, 80 (2023).
35. Rath, M., Müller, I., Kropf, P., Closs, E. I. & Munder, M. Metabolism via Arginase or Nitric Oxide Synthase: Two Competing Arginine Pathways in Macrophages. *Front. Immunol.* **5**, (2014).
36. Zhao, Y., Wang, H., Zhou, J. & Shao, Q. Glutathione Peroxidase GPX1 and Its Dichotomous Roles in Cancer. *Cancers (Basel)* **14**, 2560 (2022).
37. Brigelius-Flohé, R. & Flohé, L. Regulatory Phenomena in the Glutathione

Peroxidase Superfamily. *Antioxidants & Redox Signaling* **33**, 498–516 (2020).

38. Cruz-Gregorio, A., Aranda-Rivera, A. K., Ortega-Lozano, A. J., Pedraza-Chaverri, J. & Mendoza-Hoffmann, F. Lipid metabolism and oxidative stress in HPV-related cancers. *Free Radical Biology and Medicine* **172**, 226–236 (2021).
39. Regulatory Phenomena in the Glutathione Peroxidase Superfamily - PubMed. https://pubmed.ncbi.nlm.nih.gov/31822117/.
40. Yang, W. S. *et al.* Regulation of ferroptotic cancer cell death by GPX4. *Cell* **156**, 317–331 (2014).
41. GSTM3 enhances radiosensitivity of nasopharyngeal carcinoma by promoting radiation-induced ferroptosis through USP14/FASN axis and GPX4 - PubMed. https://pubmed.ncbi.nlm.nih.gov/38228715/.
42. Singh, H., Sachan, R., Devi, S., Pandey, S. N. & Mittal, B. Association of GSTM1, GSTT1, and GSTM3 gene polymorphisms and susceptibility to cervical cancer in a North Indian population. *Am J Obstet Gynecol* **198**, 303.e1–6 (2008).
43. Qian, J.-Y. *et al.* A prospective therapeutic strategy: GPX4-targeted ferroptosis mediators. *European Journal of Medicinal Chemistry* **281**, 117015 (2025).
44. Zois, C. E. & Harris, A. L. Glycogen metabolism has a key role in the cancer microenvironment and provides new targets for cancer therapy. *J*

Mol Med (Berl) **94**, 137–154 (2016).

45. Zhang, Y. *et al.* Stabilization of mismatch repair gene PMS2 by glycogen synthase kinase 3beta is implicated in the treatment of cervical carcinoma. *BMC Cancer* **10**, 58 (2010).
46. Gu, Z., Zhang, H., Guo, X. & Cao, Y. Enhanced Glycogen Metabolism Supports the Survival and Proliferation of HPV-Infected Keratinocytes in Condylomata Acuminata. *J Invest Dermatol* **140**, 1513-1523.e5 (2020).
47. Anacker, D. C. *et al.* HPV31 utilizes the ATR-Chk1 pathway to maintain elevated RRM2 levels and a replication-competent environment in differentiating Keratinocytes. *Virology* **499**, 383–396 (2016).
48. Moody, C. A. Impact of Replication Stress in Human Papillomavirus Pathogenesis. *J Virol* **93**, e01012-17 (2019).

Figures

Figure 1. Analysis of total metabolites in CA patients and healthy controls

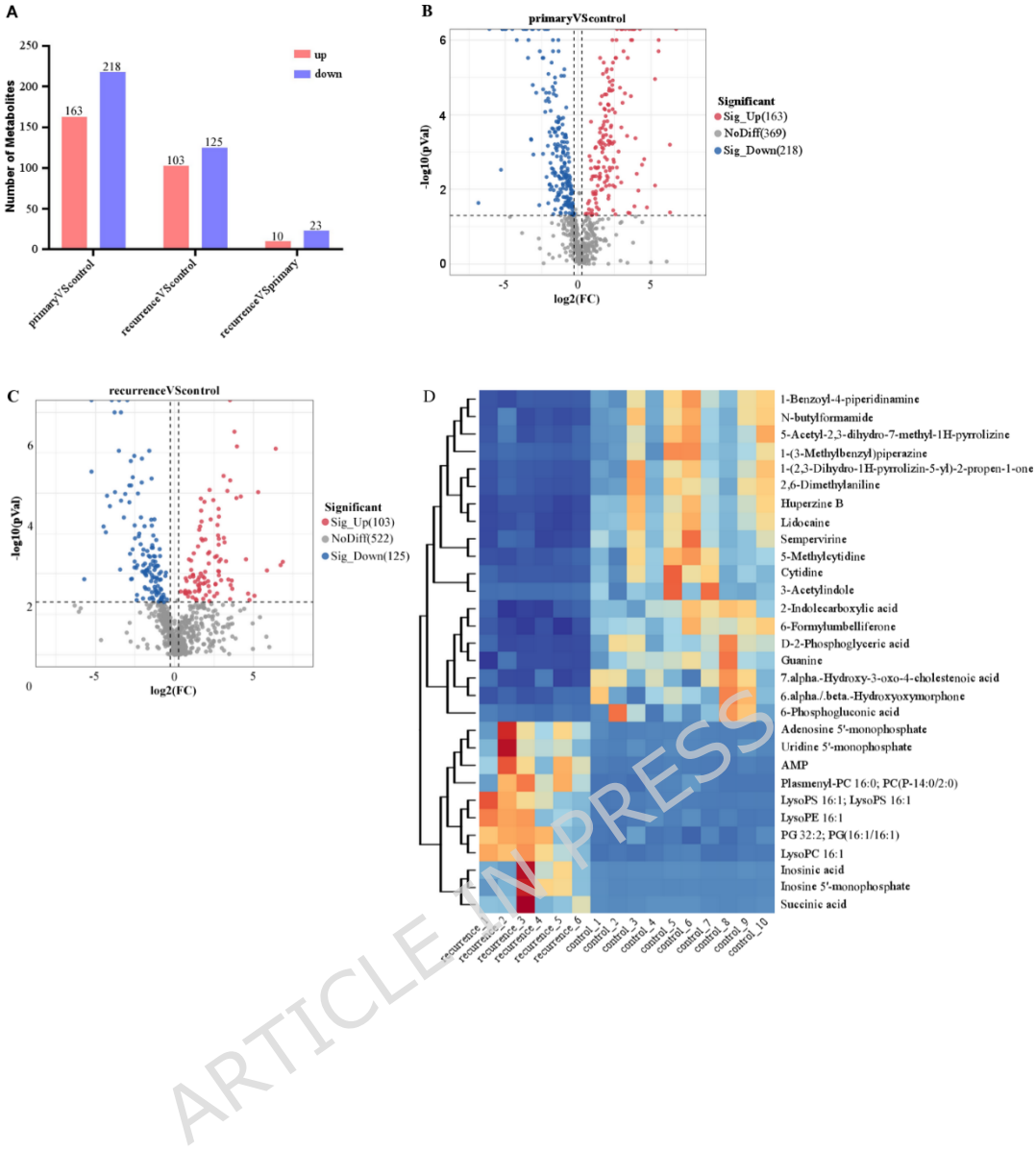

Figure 2. KEGG enrichment analysis of metabolites between recurrent CA patients and healthy controls

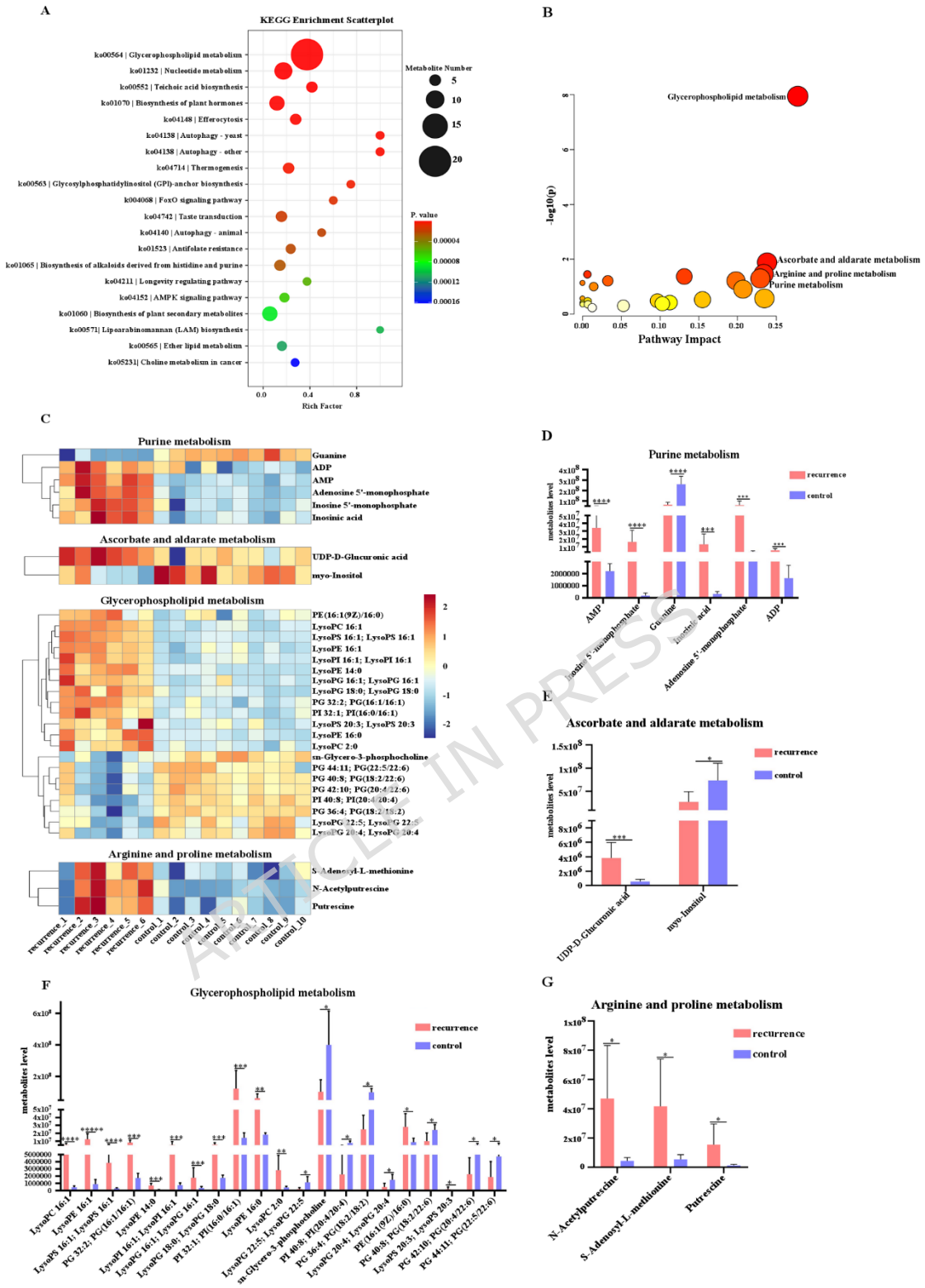

Figure 3. Single-cell sequencing of skin biopsy specimens in recurrent CA patients

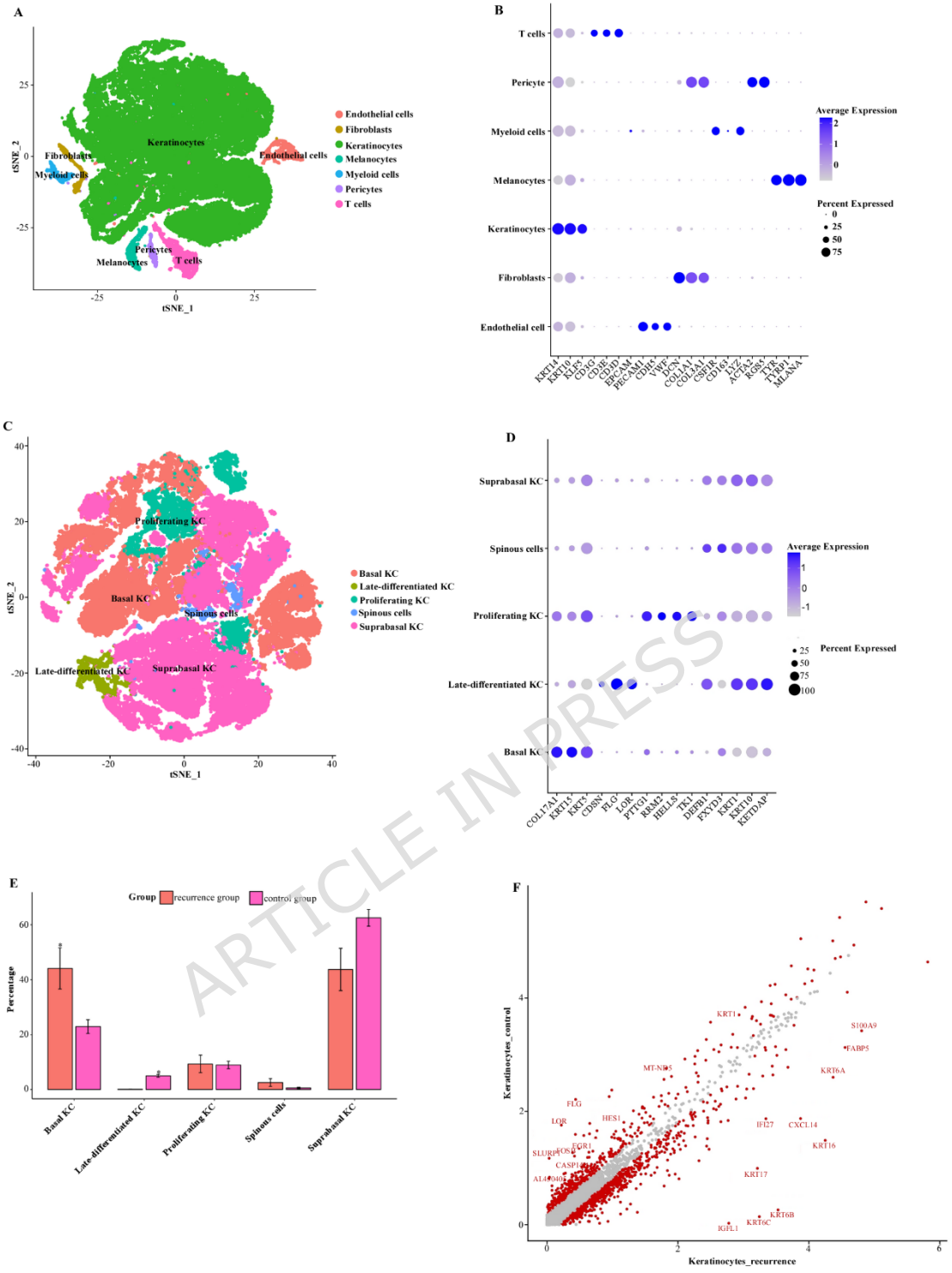

Figure 4. KEGG pathway analysis of genes expressed in KC of recurrent CA patients

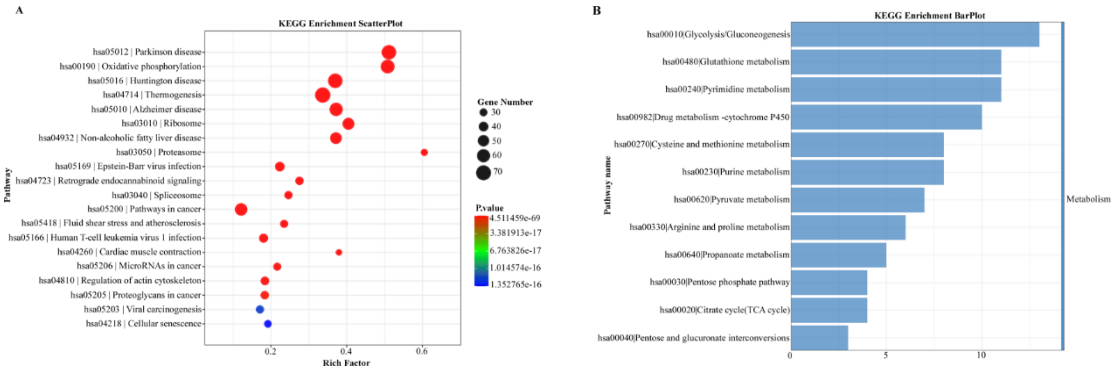

Figure 5. Gene expression changes in glycolysis/gluconeogenesis, glutathione, and pyrimidine metabolism in KC of recurrent CA patients

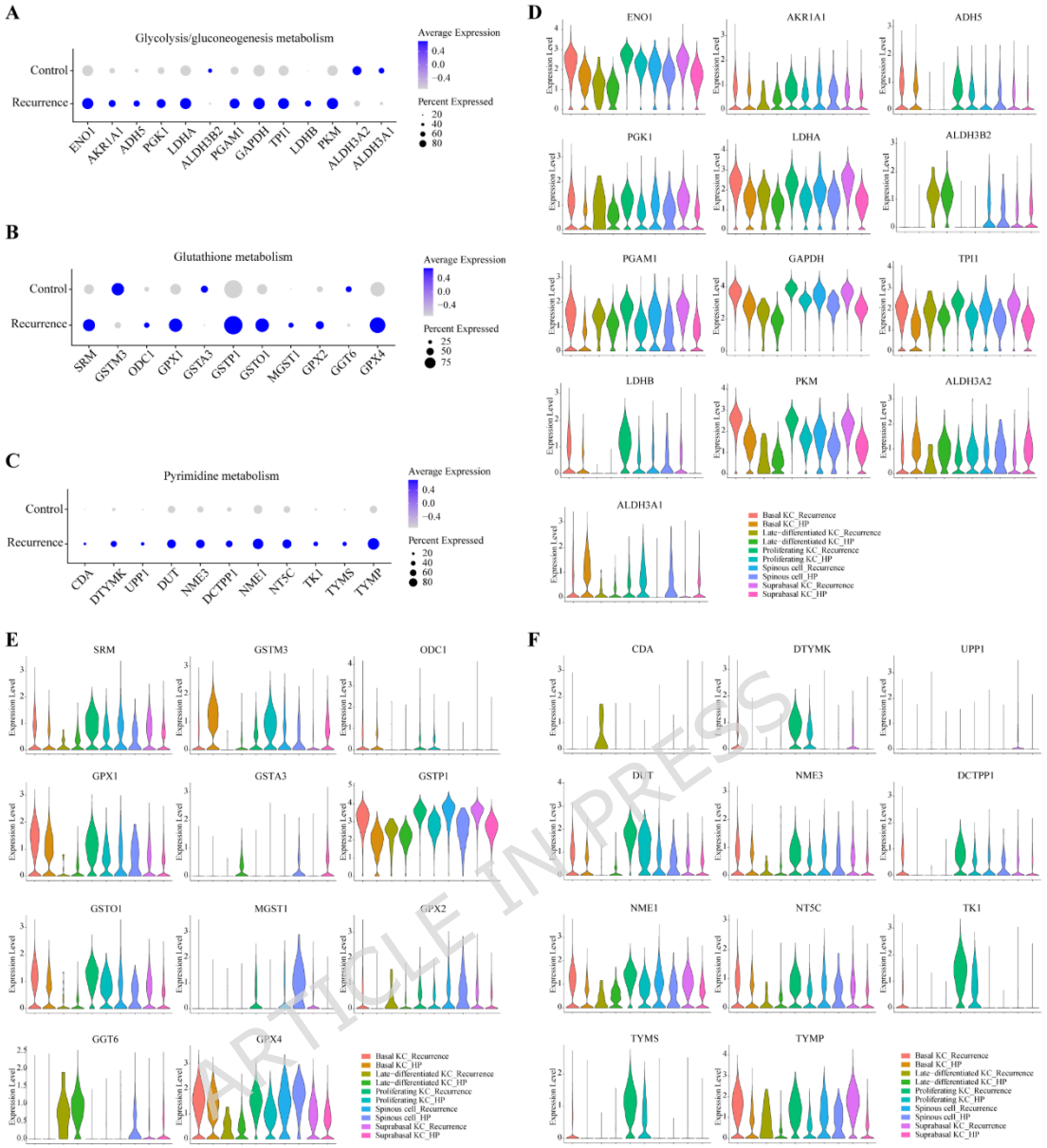

Figure 6. Gene expression changes in arginine and proline metabolism, purine metabolism in KC of recurrent CA patients

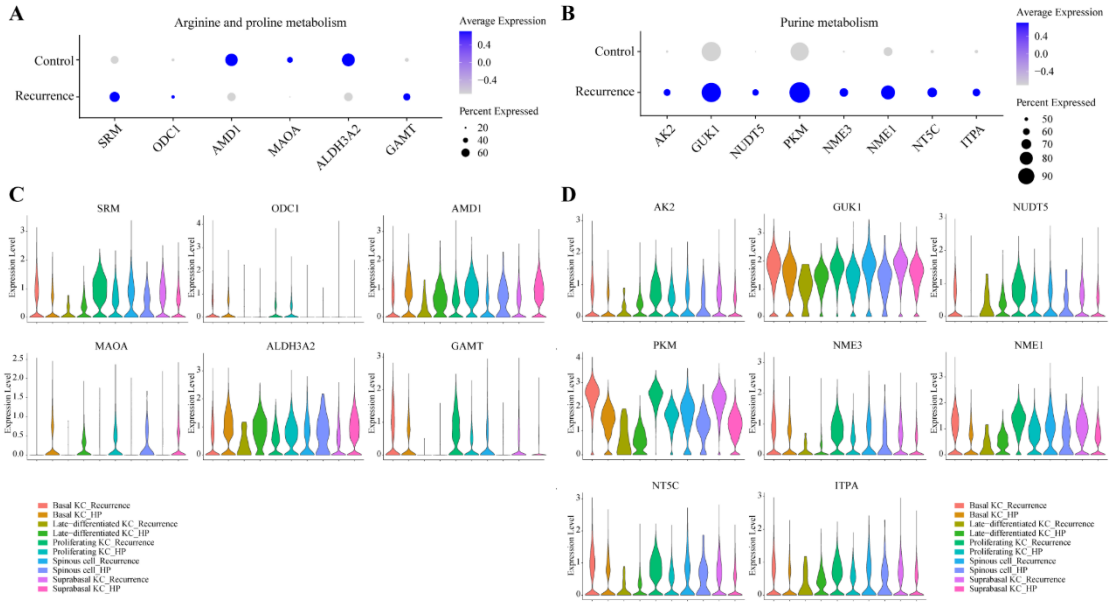

Figure 7. Single-cell analysis reveals M2 macrophage and dendritic cell dysfunction associated with recurrent CA

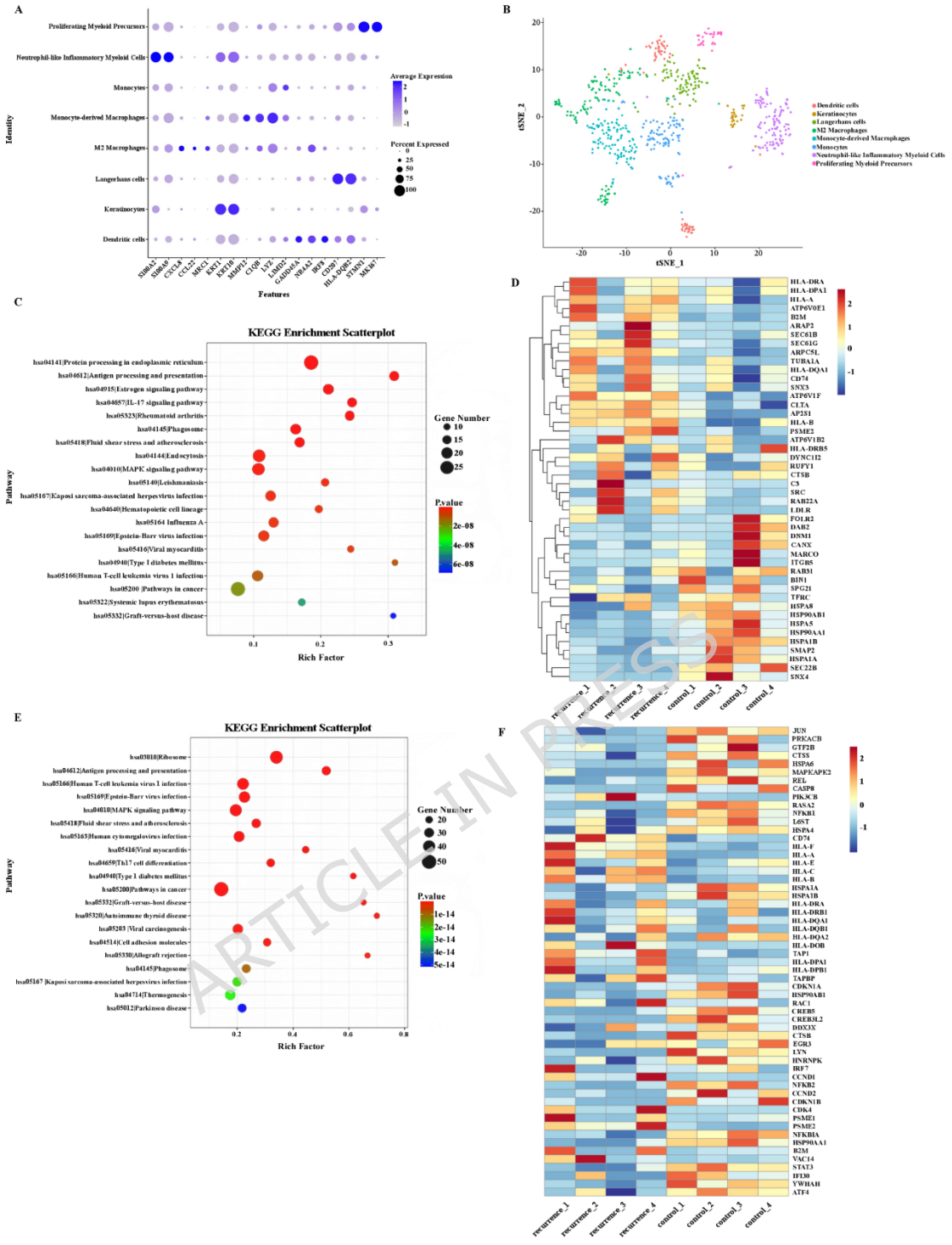

Figure 8. Immunohistochemical and immunofluorescence analysis of AMD1, GSTM3, ALDH3A1, GPX4, and RRM2

expression in recurrent CA patients

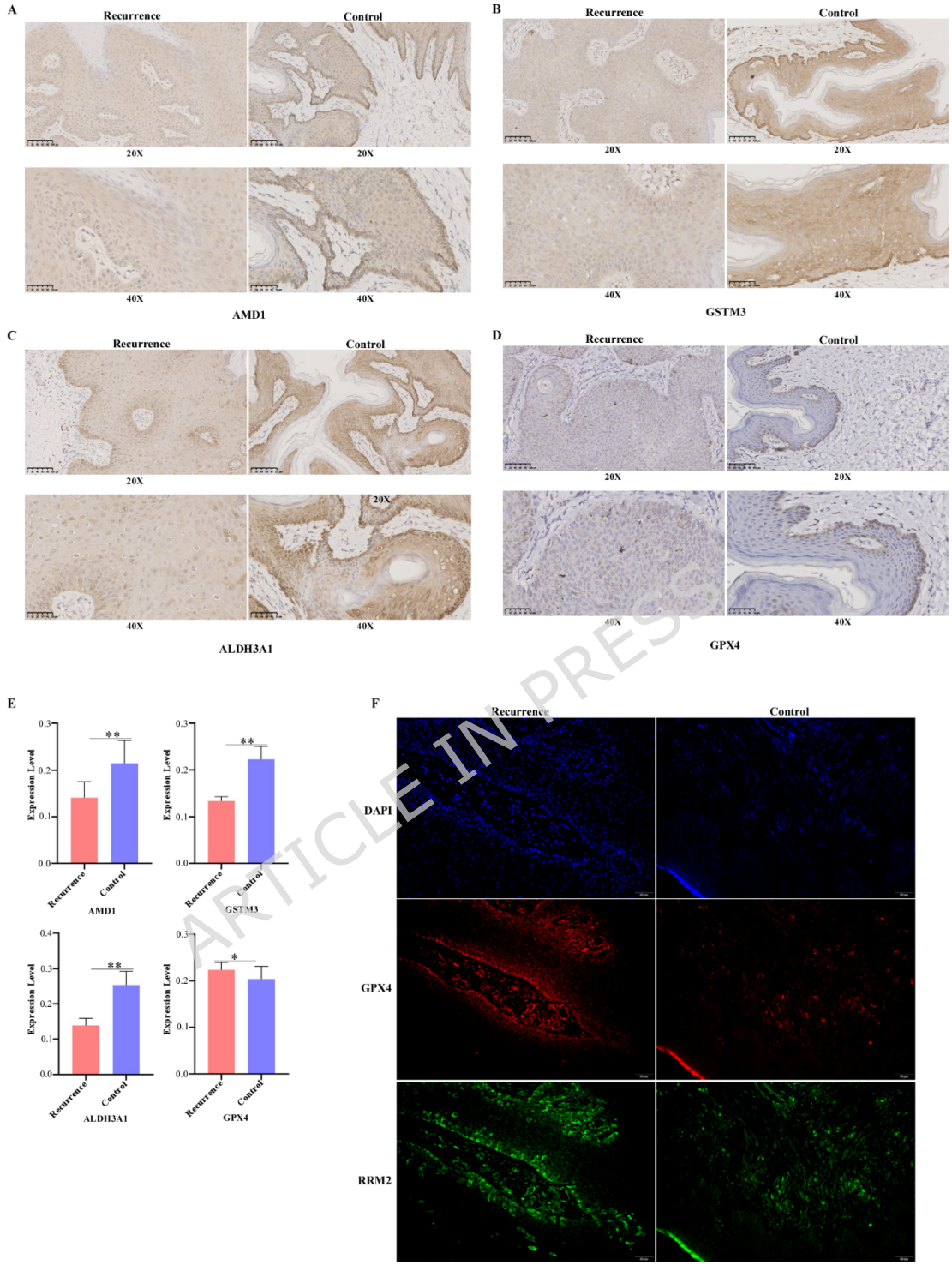

Figure legends

Figure 1. Analysis of total metabolites in CA patients and healthy controls

(A) Bar graph depicting the differentially regulated metabolites in CA samples compared to healthy controls.

(B) Volcano plot illustrating the differential metabolites expression between primary CA patients and healthy controls, as identified through metabolomic analysis.

(C) Volcano plot showing the differential metabolite expression between recurrent CA patients and healthy controls, as determined by metabolomic profiling.

(D) Heatmap displaying the 30 most significantly altered metabolites in recurrent CA patients compared to healthy controls.

Figure 2. KEGG enrichment analysis of metabolites between recurrent CA patients and healthy controls

(A) Enrichment analysis of the metabolites sets in skin tissues in recurrent CA patients compared to healthy controls.

(B) Pathway analysis of the most significantly altered metabolites in skin tissues in recurrent CA patients compared to healthy controls.

(C-G) Heat map **(C)** and bar graph showed the most dramatically altered metabolites associated with purine metabolism **(D)**, ascorbate and aldarate metabolism **(E)**, glycerophospholipid metabolism **(F)**, and arginine and proline metabolism **(G)**. $*p < 0.05$, $**p < 0.01$, $***p < 0.001$.

Note: Some KEGG pathway names (e.g., “Biosynthesis of plant hormones” and “Autophagy-yeast”) refer to evolutionarily conserved enzymatic modules and therefore represent shared metabolic processes in human cells rather than nonhuman biological pathways.

KEGG pathway maps were obtained from the KEGG database[22–24].

Figure 3. Single-cell sequencing of skin biopsy specimens in

recurrent CA patients

(A)t-SNE plot of single-cell RNA sequencing from skin biopsies of four recurrent CA patients and four healthy controls, revealing seven distinct cell types: keratinocytes, T cells, endothelial cells, fibroblasts, myeloid cells, pericytes, and melanocytes.

(B) Dot plot showing the expression of discriminatory markers for each cell type cluster, with average expression (indicated by blue intensity) and expression frequency (circle size).

(C)t-SNE plot depicting five keratinocyte subgroups—basal, late-differentiated, proliferating, spinous, and suprabasal—each characterized by specific gene expression.

(D) Marker gene expression profiles for the five keratinocyte subgroups, with average expression (blue intensity) and expression frequency (circle size).

(E) Comparison of keratinocyte subgroup proportions, showing a significant increase in basal keratinocytes (p = 0.028) and a decrease in late-differentiated keratinocytes (p = 0.028) in recurrent CA patients.

(F) Scatter plot of differentially expressed metabolism-related genes between recurrent CA patients and controls, highlighting significantly altered genes.

Figure 4. KEGG pathway analysis of genes expressed in KC of recurrent CA patients

(A)KEGG pathway analysis highlighting enriched pathways associated with genes expressed in KC.

(B) Bar graph showing the twelve most significantly altered pathways in keratinocytes, with the glycolysis / gluconeogenesis signaling pathway, glutathione metabolism, and pyrimidine metabolism identified as the top three metabolic pathways affected.

Note: Some enriched pathway names (e.g., “Parkinson’s disease”, “Huntington’s disease”) reflect conserved mitochondrial and proteasomal gene modules in KEGG and do not imply non-skin or neuron-specific biological processes.

KEGG pathway maps were obtained from the KEGG database[22–24].

Figure 5. Gene expression changes in glycolysis/gluconeogenesis, glutathione, and pyrimidine metabolism in KC of recurrent CA patients

(A) Scatter plot illustrating expression of glycolysis / gluconeogenesis-related genes in KC in recurrent patients compared with controls. 10 genes were significantly up-regulated, while 3 genes were significantly down-regulated.

(B) Scatter plot illustrating expression of glutathione metabolism-related genes in KC in recurrent patients compared with controls. 8 genes were significantly up-regulated, while 3 genes were significantly down-regulated.

(C) Scatter plot illustrating expression of pyrimidine metabolism-related genes in KC in recurrent patients compared with controls. 11 genes were significantly up-regulated.

(D) Violin plot showing the expression of glycolysis / gluconeogenesis-related genes in KC between recurrent patients and controls

(E) Violin plot showing the expression of pyrimidine metabolism-related genes in KC between recurrent patients and controls.

(F) Violin plot showing the expression of glutathione metabolism-related genes in KC between recurrent patients and controls.

Figure 6. Gene expression changes in arginine and proline metabolism, purine metabolism in KC of recurrent CA patients

(A) Scatter plot illustrating expression of arginine and proline metabolism-related genes in KC in recurrent patients compared with controls.3 genes were significantly up-regulated, while 3 genes were significantly down-regulated.

(B) Scatter plot showing the expression of purine metabolism-related genes across different keratinocyte subclusters.

8 genes were significantly up-regulated.

(C) Violin plot showing the expression of arginine and proline metabolism-related genes in KC between recurrent patients and controls.

(D) Violin plot showing the expression of purine metabolism-related genes across different keratinocyte subclusters.

Figure 7. Single-cell analysis reveals M2 macrophage and dendritic cell dysfunction associated with recurrent CA

(A) Dot plot of marker gene expression across cell clusters, with average expression (blue intensity) and frequency (circle size).

(B)t-SNE plot showing seven myeloid cell subgroups: dendritic cells, Langerhans cells, M2 macrophages, monocyte-derived macrophages, monocytes, neutrophil-like inflammatory myeloid cells, and proliferating myeloid precursors.

(C) Enrichment analysis of the genes expressed in M2 macrophages from recurrent CA patients compared to healthy controls.

(D) Heatmap of significantly altered genes in M2 macrophages between recurrent CA patients and healthy controls.

(E) Enrichment analysis of genes expressed in dendritic cells from recurrent CA patients compared with healthy controls.

(F) Heatmap of the significantly altered genes in dendritic cells between recurrent CA patients and healthy controls.

Note: KEGG pathway maps were obtained from the KEGG database[22–24].

Figure 8. Immunohistochemical and immunofluorescence analysis of AMD1, GSTM3, ALDH3A1, GPX4, and RRM2 expression in recurrent CA patients

(A) Representative immunohistochemistry staining of AMD1 in recurrence CA patients and healthy controls. Scale bar, 20X, 100 μm; 40X, 50 μm.

(B) Representative immunohistochemistry staining of GSTM3 in recurrence CA patients and healthy controls. Scale bar, 20X, 100 μm; 40X, 50 μm.

(C) Representative immunohistochemistry staining of ALDH3A1 in recurrence CA patients and healthy controls. Scale bar, 20X, 100 μm; 40X, 50 μm.

(D) Representative immunohistochemistry staining of GPX4 in recurrence CA patients and healthy controls. Scale bar, 20X, 100 μm; 40X, 50 μm.

(E) Quantitative analysis of the expression of AMD1, GSTM3, ALDH3A1, and GPX4 between CA patients and healthy controls, $^{**}p < 0.01$, $^{*}p < 0.05$.

(F) Representative immunofluorescence staining of DAPI, GPX4 and RRM2 in recurrence CA patients and healthy controls, Scale bar, 40X, 50 μm.